Microwave-assisted optimization of the manganese redox states for enhanced capacity and capacity retention of LiAl$_x$Mn$_{2-x}$O$_4$ (x = 0 and 0.3) spinel materials†

Funeka P. Nkosi,[ab] Charl J. Jafta,[b] Mesfin Kebede,[b] Lukas le Roux,[b] Mkhulu K. Mathe[b] and Kenneth I. Ozoemena*[abc]

Microwave irradiation at the pre- and post-annealing steps of the synthesis of LiAl$_x$Mn$_{2-x}$O$_4$ (x = 0 and 0.3) spinel cathode materials for rechargeable lithium ion batteries is a useful strategy to optimize the average manganese valence number (n_{Mn}) for enhanced capacity and capacity retention. The strategy impacts on the lattice parameter, average manganese valence, particle size and morphology, reversibility of the de-intercalation/intercalation processes, and capacity retention upon continuous cycling. Microwave irradiation is able to shrink the particles for improved crystallinity. The XPS data clearly suggest that microwave irradiation can be used to tune the manganese valence (n_{Mn}), and that the LiAl$_x$Mn$_{2-x}$O$_4$ with $n_{Mn} \approx 3.5+$ gives the best electrochemical performance. These new findings promise to revolutionize how we use microwave irradiation in the preparation of energy materials and various other materials for energy storage and conversion materials for enhanced performance.

Introduction

Rechargeable lithium ion batteries (RLIBs) have proved themselves as the most attractive advanced battery technologies for electric vehicles and portable electronics.[1–8] Perhaps, the lithium manganese oxide, LiMn$_2$O$_4$ (LMO) spinel material needs little or no introduction as it has proved itself as one of the most attractive cathode materials for RLIBs due to its high operating voltage (4 V), low cost, environmental compatibility, and stability at low temperature compared to other cathode materials.[5,9–11] LMO has begun to show some commercial success; it is the cathode material that drives Nissan Leaf (a pure electric vehicle) and Chevrolet Volt (a plug-in hybrid electric vehicle). Despite the advantages of LMO, one of its major challenges that still conspire against its full utilization is capacity fading upon continuous cycling. The capacity loss is caused by two main factors, the so-called Jahn–Teller distortion and slow dissolution of manganese in the electrolyte.[12,13] The Jahn–Teller effect is the reduction of the crystal symmetry from cubic to tetragonal structure, and it is this structural transition

that deteriorates its cycle life and is said to occur when the average manganese valence number (n_{Mn}) is equal or less than 3.5.[14,15] The stress generated by this phenomenon leads to cracking of particles and loss of electric contact upon cycling. The manganese ions in LMO are believed to exist as 50% Mn^{3+} and 50% Mn^{4+} (*i.e.*, n_{Mn} = 3.5+). High content of Mn^{3+} ions causes capacity fading, and leads to the dissolution of the cathode material into the electrolyte.

There are three known strategies for improving the cycling performance of LMO; (i) making the spinel structure lithium-rich (Li-excess),[16–18] (ii) doping with cations[19–21] and (iii) coating with metal oxides. Aluminium is a preferred dopant for LMO[16–18] since it is abundant, non-toxic, less expensive and lighter than transition metal elements. Reports on the application of microwave irradiation (MWI) in the preparation of LMO have focussed on reducing the synthesis time,[22–28] there is no report on the strategic utilisation of MWI aimed at curbing the recalcitrant capacity fading. We have found that microwave irradiation can enhance cycling behaviour by controlling the manganese valence state, structure, and morphological integrity of the LMO and Al-doped LMO. In a nutshell, the MWI is a viable 'curative' treatment to LMO powder to enhance its capacity retention.

Experimental procedure

Chemicals and materials

Lithium nitrate (LiNO$_3$), manganese nitrate tetrahydrate (Mn(NO$_3$)$_2$·4H$_2$O), urea (CO (NH$_2$)$_2$) and aluminum nitrate

[a]*Department of Chemistry, University of Pretoria, Pretoria 0002, South Africa. E-mail: kozoemena@csir.co.za; Fax: +27 128412135; Tel: +27 128413664*

[b]*Energy Materials, Materials Science and Manufacturing, Council for Scientific & Industrial Research (CSIR), Pretoria 0001, South Africa*

[c]*School of Chemistry, University of the Witwatersrand, Private Bag 3, P O WITS 2050, Johannesburg, South Africa*

nonahydrate ($Al(NO_3)_2 \cdot 9H_2O$), carbon black, N-methyl-2-pyrrolidone (NMP), polyvinylidene fluoride (PVDF), lithium metal (50 μm thick), lithium hexafluorophosphate ($LiPF_6$), ethylene carbonate (EC), diethyl carbonate (DEC), and dimethyl carbornate (DMC) were purchased from Sigma-Aldrich and used without further purification. Aluminum foil (50 μm thick) was obtained from MTI Corporation, USA.

Synthesis of LMO and Al-doped LMO powders

LMO-based powders were obtained from the nitrate salts of Li and Mn *via* the combustion method with urea as the fuel. $LiNO_3$ (1.10 g, 0.016 mol), $Mn(NO_3)_2 \cdot 4H_2O$ (8.00 g, 0.032 mol) and urea (2.87 g, 0.047 mol) were dissolved in deionised water (20.00 ml) and stirred until the starting materials were completely dissolved. The resultant solution was heated in the furnace at 550 °C for ~7 min to yield a black powder product. This sample was divided into three portions. The first portion was annealed at 700 °C for 10 h using a tube furnace (50 mm, MTI Corporation). The LMO powder obtained by this conventional annealing process is abbreviated as LMO-a. The second portion was subjected to microwave irradiation at 600 W for 20 min (using the Anton Paar Multiwave 3000 system, $\lambda = 0.12236$ m) and then annealed at 700 °C for 10 h (abbreviated as LMO-ma). The third portion was first annealed at 700 °C for 10 h and then subjected to microwave irradiation as described above (abbreviated as LMO-am). The aluminum-doped LMO ($LiMn_{1.7}Al_{0.3}O_4$) were prepared using the same procedure as for the LMO-based samples. The $LiMn_{1.7}Al_{0.3}O_4$ powders were prepared using 1.10 g $LiNO_3$, 6.80 g $Mn(NO_3)_2 \cdot 4H_2O$, 1.80 g $Al(NO_3)_2 \cdot 9H_2O$ and 2.87 g urea. The powders were similarly named LMOA-a, LMOA-am and LMOA-ma. The schematic of the procedure is summarized in Fig. 1. We attempted 10 and 20 min duration at 600 W treatments for LMO-ma and got better XRD pattern for the 20 min duration than for the 10 min, hence 20 min was used for all subsequent microwave experiments.

Materials characterization

Scanning electron microscopic micrographs were acquired using a LEO 1525 field emission scanning microscope (FE-SEM)
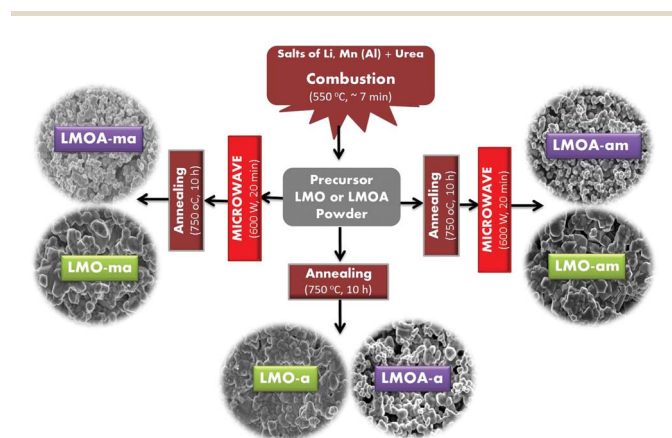
with the acceleration voltage of 200 kV. HRTEM measurements were carried out on a Joel HRJEM-2100 microscopy using LAB6 filament as an electron source. The measurements were carried out using electron beam at 200 kV. Powder XRD data were acquired using a PANalytical X'Pert Pro diffractometer with CuKα radiation, $\lambda = 1.5046$ Å as a radiation source operating at 45 kV and 40 mA, scan range between 5 and 90°. XPS measurements were carried out using Kratos Axis Ultra-DLD system (Shimadzu) with Al Kα radiation (1486.6 eV). The binding energy was calibrated with reference to the C 1s level of the carbon (284.6 eV). The FTIR spectra were recorded using a Perkin Elmer Spectrum 100 FTIR spectrometer in the range 400–4000 cm^{-1}. The analysis was carried out using a diamond crystal probe and air was used as a background. Pellets of the samples were mixed with KBr in the ratio 1 : 3 and prepared by the disk method. The pellets were made using a thickness that provided good transparency for IR radiation. Raman measurements were carried out in air using a Horiba Jobin Yvon spectrometer equipped with 10× objective lens to focus the laser beam on a small selected area of the sample, a 30 mW green argon laser ($\lambda = 514$ nm) an excitation source, and a 1800 lines per mm grating monochromator with an air-cooled CCD detector. Raman spectra were measured up to 1000 cm^{-1} on the stokes side, with a spectral resolution of about 3 cm^{-1}.

Fabrication of coin cells and electrochemical characterization

The cathodes for the electrochemical studies were prepared by making up of slurry which contained 80% of the LMO powders mixed with 10% carbon black and 10% polyvinylidene fluoride (PVDF) binder in N-methyl-2-pyrrolidone (NMP) as the solvent. The slurry was applied using a doctor-blade method onto an aluminium foil as a current corrector. The coated aluminium foil was dried under vacuum at 110 °C for 12 h, then pressed to form a uniform

Fig. 1 Schematic representation of the microwave-assisted combustion synthesis of $LiMn_2O_4$ (LMO) and $LiMn_{1.7}Al_{0.3}O_4$ (LMOA). The abbreviations are as described in the experimental section.
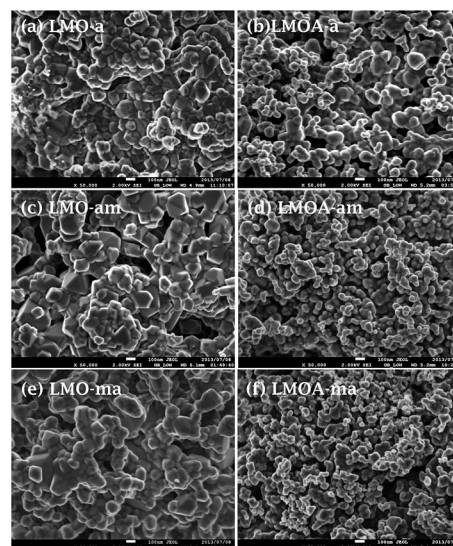

Fig. 2 Typical FE-SEM micrographs of LMO powders at low magnifications (100 nm). The abbreviations are as described in Fig. 1.
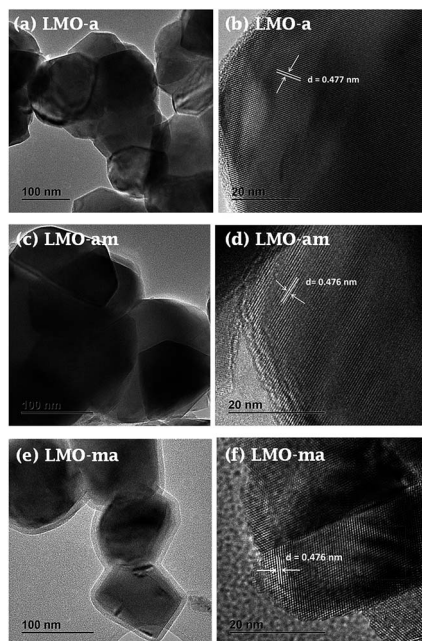
Fig. 3   Typical TEM and HRTEM images of LMO-based powders.

layer. The electrodes were heated at 80 °C under vacuum for at least 6 h, and then kept in the glovebox (MBRAUN MB10 compact) for 2 h before the fabrication of the coin cells. The coin cells (type CR 2032) composed of the positive electrode (cathode) made from the required spinel LMO powder, lithium metal as the negative electrode (anode) and a Celgard polypropylene-based membrane separator soaked in non-aqueous electrolyte. A 1 M $LiPF_6$ in EC/DC/DMC in 1 : 1 : 1 volume ratio solution was used as the electrolyte. $LiPF_6$ in EC–DMC–DEC has increased ion mobility and high ionic conductivity compared to a commercial electrolyte with $LiPF_6$ in EC/DEC. High conductivity of the electrolyte will minimize the internal resistance of the cell.

The coin cells also contained a stainless steel spacer to provide an electrical connection from the electrode to the case, and a spring to exert pressure on the components to allow maximum contact of the cathode and anode when the coin cell is sealed. The coin cells were assembled in a glovebox filled with ultra-high purity argon gas with the concentration of H_2O and O_2 maintained at <0.5 ppm. The electrolyte was left in the glove box overnight before being used to fabricate the coin cells. After all components of the coin cells were aligned, the coin cell was sealed with a Compact Hydraulic Crimping Machine (MSK-110). The pressure on the crimper was set at 750 psi to seal the coin cells. After fabrication, the coin cells were allowed to stand for 24 h before the electrochemical measurements were performed. Cyclic voltammetry (CV) was conducted at a scan rate of 0.1 mV s^{-1} over a range of 3.5–4.3 V using a Bio-Logic science VMP3-based instrument using the EC-lab V10.32 software. The charge–discharge capacity and cycle performance (rate capability) were measured at different C-rates (charge–discharge rates) between 3.5 and 4.3 V using a Maccor 4000 battery tester.
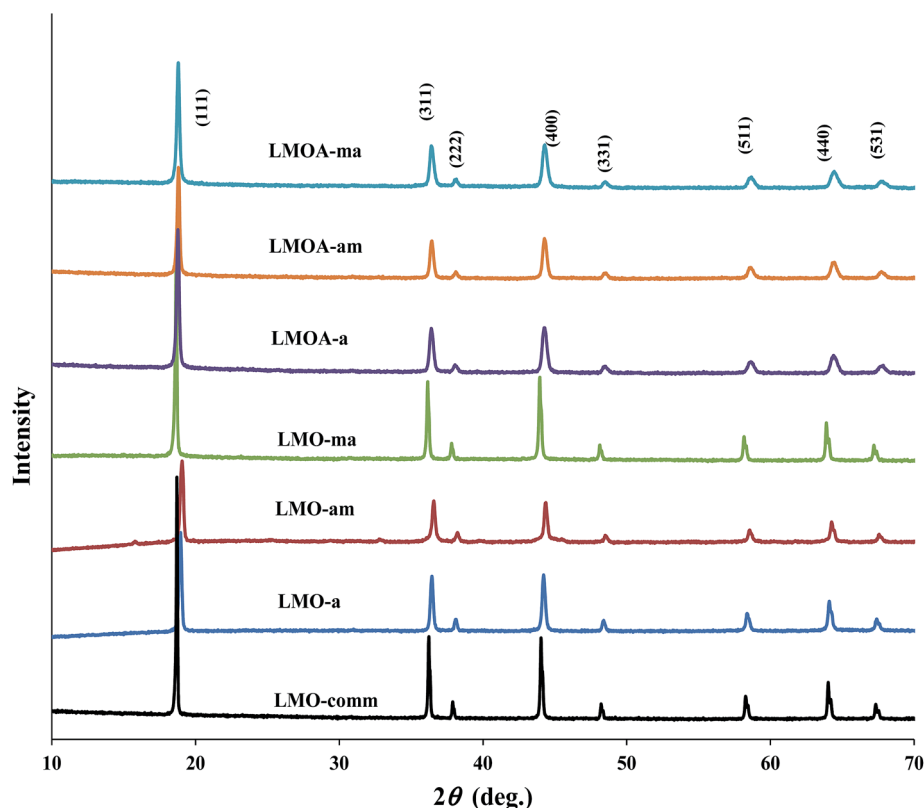

Fig. 4   Typical powder XRD patterns of the LMO- and LMOA-based powders.

Table 1 XRD, XPS (Mn-2p$_{3/2}$ spectra) and electrochemical data of the LMO and LMOA based samples

Sample	XRD data	Binding energy position (eV)		Cation distribution			Coin cell data	
	Lattice parameter (Å)	Mn^{4+}	Mn^{3+}	Mn^{4+} (%)	Mn^{3+} (%)	Mn valence (n_{Mn})	Initial capacity (mA h g^{-1})	Capacity loss after 50 cycles
LMO-a	8.2565 ± 0.0010	644.5	642.2	16.5	83.5	3.165	127.5	22.0%
LMO-am	8.2441 ± 0.0012	645.8	642.7	49.7	50.3	3.498	94.3	9.0%
LMO-ma	8.2403 ± 0.0012	646.5	644.6	54.2	45.8	3.541	131.5	5.0%
LMO-comm	8.2161 ± 0.0012	644.1	642.6	40.1	59.9	3.400	—	—
LMO[29]	8.2404 ± 0.0013	—	—	51	49	3.503	118.6	66.8%
LMOA-a	8.1701 ± 0.0011	644.4	642.4	31.0	69.0	3.310	95.3	7.2%
LMOA-am	8.1671 ± 0.0011	644.5	642.8	49.2	50.8	3.493	103.6	0.4%
LMOA-ma	8.1696 ± 0.0011	644.3	642.6	31.2	68.8	3.312	73.6	0.7%
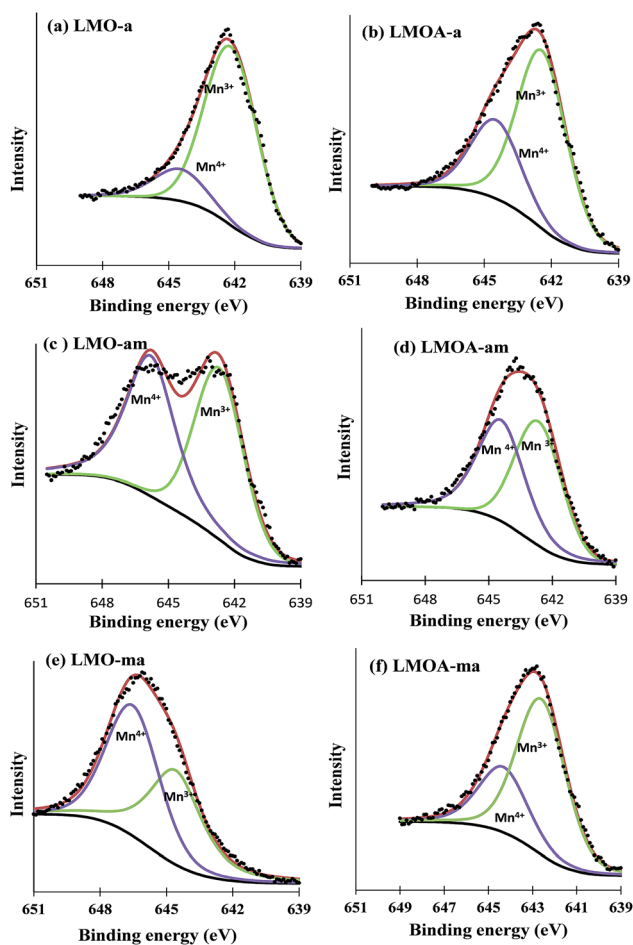
Fig. 5 XPS Mn 2p$_{3/2}$ spectra of LMO- and LMOA-based samples.

All of the electrochemical performance measurements were carried at room temperature.

Results and discussion

Morphological and structural characterization

The FESEM images of the spinel materials at low magnification are shown in Fig. 2 (also see ESI, Fig. S1† for high magnification). The LMOA samples are smaller in size (10–130 nm) than the LMO samples (80–250 nm) or the commercial LMO sample (LMO-comm, ≥1 μm, ESI, Fig. S2†). From the comparative TEM images of the LMO-based samples (Fig. 3) and the LMOA-based samples (ESI, Fig. S3†), the spinels are crystalline, with well-defined lattice fringes, and an average *d*-spacing of 0.473 ± 0.04 nm which confirm the (111) plane in the lattice structure. The TEM image of LMO-ma (Fig. 3e) seems to show some ultrathin coating of the particles. Considering that we did not do any coating, we can speculate that this 'coating-like' structure may be due to surface segregation due to microwave, or due to the difference in the crystallinity of the surface and bulk materials. Further experiments are necessary to confirm this observation.

The powder XRD patterns for the LMO and LMOA (Fig. 4) showed well-developed diffraction peaks of pure spinel LiMn$_2$O$_4$ and LiAl$_{0.3}$Mn$_{1.7}$O$_4$ materials. The peaks were indexed to the characteristic diffractions of spinel LiMn$_2$O$_4$ (JCPDS File no. 88-1749) with space group $Fd\bar{3}m$, corresponding to the (111), (311), (222), (400), (331), (551), (440), and (531) planes. The lattice parameter values were determined by Rietveld analysis using the Expo2013 software. Table 1 summarises the values of the lattice parameter with some interesting information when compared to commercial LMO and literature.[29] First, the LMO-a shows the largest lattice parameter, which decreased upon microwave irradiation and/or doping with aluminium. The lattice contraction means a decrease in the Mn^{3+} and increase in the Mn^{4+} ion (since the radius of Mn^{3+} (0.66 Å)) is greater than that of Mn^{4+} (0.60 Å).[30] Second, there is a dramatic contraction of the lattice parameters for the LMOA samples which is due to the fact that the radius of Mn^{3+} is greater than that of Al^{3+} (0.53 Å), and the bond length of Mn–O (1.90 Å) is longer than that of Al–O (1.62 Å); as Al^{3+} substitutes Mn^{3+} in the 16d site of spinel structure, the unit cell shrinks. In general, the lattice contraction increases the structural stability of the spinel, which is beneficial to the suppression of Jahn–Teller distortion.

XPS is a well-known surface-sensitive technique for the quantification of cations in oxide materials including spinels.[31–39] From the Mn 2p$_{3/2}$ spectra of the spinel materials (Fig. 5), the Mn^{3+}/Mn^{4+} ratio and valence number (Table 1) corroborate the lattice contraction observed in the XRD. Interestingly, the increased
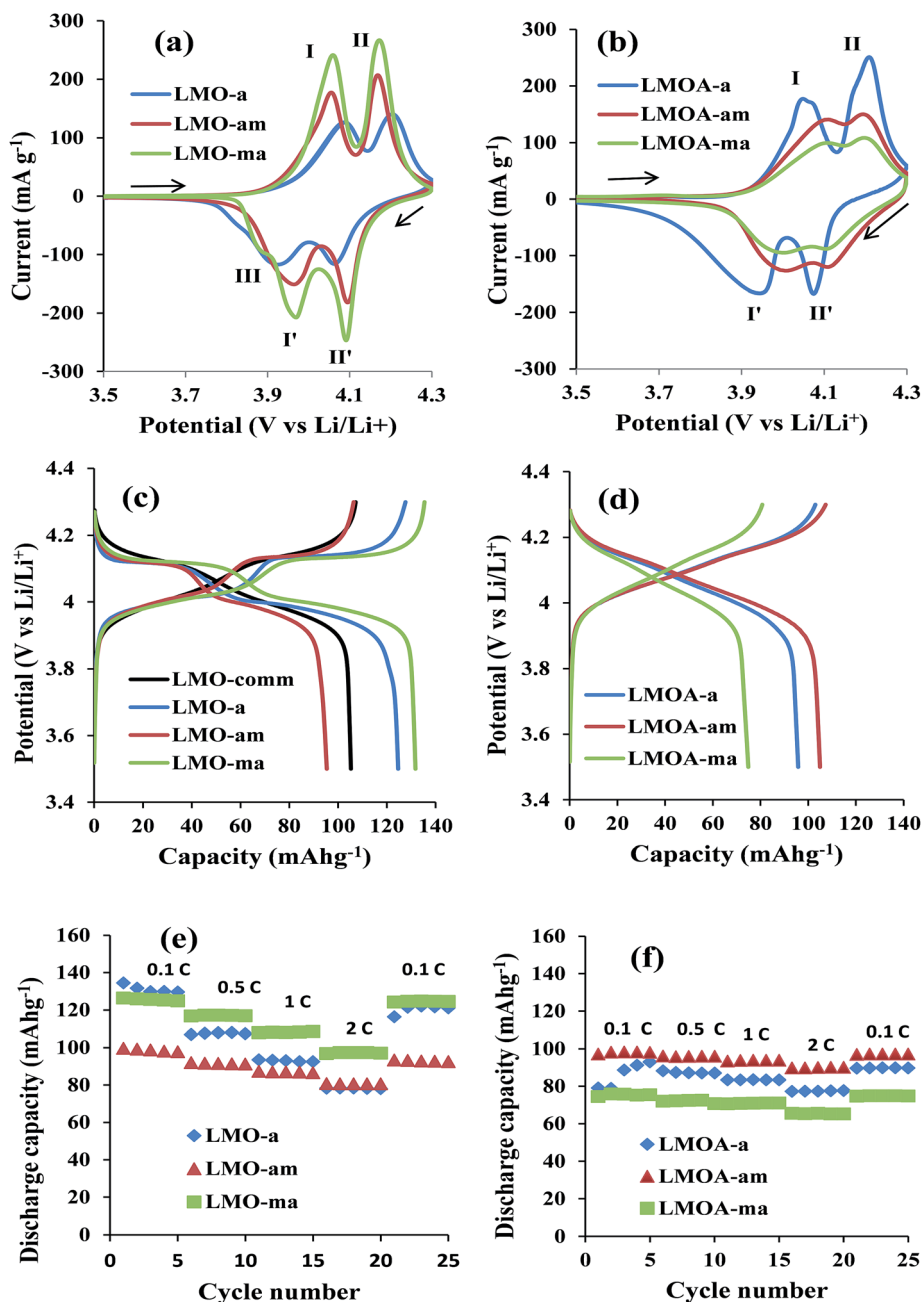
Fig. 6 Cyclic voltammograms of LMO (a) and LMOA (b) coin cells at 0.1 mV s^{-1}; galvanostatic charge–discharge of LMO (c) and LMOA (d) coin cells at 0.1 C; plots of discharge capacity *vs.* cycle number for the LMO (e) and LMOA (f) coin cells at different current densities (0.1–2 C) between 3.5 and 4.3 V range.

valence states for LMO-ma ($n_{Mn} = 3.541+$) and LMOA-am ($n_{Mn} = 3.493+$) are consistent with the slight positive shifts of their Mn-2p$_{3/2}$ binding energies compared to un-microwaved samples. Note that the n_{Mn} values for LMO-a and LMO-comm are less than 3.5+ (*i.e.*, amount of Mn^{3+} is higher than that of the Mn^{4+}) contradicting the general notion that LMO powders should be $n_{Mn} \approx 3.5+$ (*i.e.*, that the amount of Mn^{3+} is always equal to that of the Mn^{4+}). Perhaps, more interesting is that when the LMO-a was subjected to microwave irradiation to obtain the LMO-am, we observed a lattice shrinkage (from 8.256 to 8.244 Å) leading to $n_{Mn} \approx 3.5+$. This

result strongly proves that our microwave irradiation strategy is able to convert excess Mn^{3+} to Mn^{4+} to generate the expected $n_{Mn} \approx 3.5+$ value. The microwave-treated samples with $n_{Mn} \approx 3.5+$ (LMO-ma and LMOA-am) exhibited the strongest Raman and IR peaks (ESI, Fig. S4†), confirming the effect of the microwave irradiation in strengthening the Mn–O bonding for enhanced electrochemistry. The LMOA samples showed positive peak shifts (≥ 20 cm^{-1}), which indicates a relatively stronger bonding in the Mn(Al)O$_6$ octahedra due to Al-doping and the microwave irradiation.

The electrochemistry of the coin cells was studied as shown in Fig. 6. The cyclic voltammetric evolutions of the LMO and LMOA-based coin cells (Fig. 6a and b) showed two redox couples (I/I′ and II/II′), indicating an expected two-step lithium ion insertion/extraction reactions.[40] The shoulder peak *ca.* 3.874 V (peak III) of the LMO-ma is attributed to the 'formation cycle' during initial cycles whereby minor structural rearrangement of the lattice takes occur.[41] From the CV data (summarised in ESI, Table S1†) clearly indicate reversibility of the redox processes, with the microwave-treated samples showing enhanced reaction kinetics compared to the un-microwaved samples. The discharge capacities (Fig. 6c and d) for the LMOA based coin cells are lower than that of un-doped LMO sample due to the replacement of the redox-active Mn^{3+} with redox-inactive Al^{3+} in the spinel structure. From the rate capability studies (Fig. 6e and f) the microwave-treated samples (LMO-am, LMOA-am and LMOA-ma) gave higher capacities at high C-rates and showed almost the same capacity when returned to the initial 0.1 C-rate compared to the standard LMO and LMOA-based coin cells.

There are critical findings from the coin cell data in Table 1 (also from discharge capacity *vs.* cycle number *vs.* coulombic efficiency curves in ESI, Fig. S5†) that should be emphasized. First, the LMO obtained by a short microwave exposure prior to annealing (*i.e.*, LMO-ma materials with $n_{Mn} \approx 3.5+$) gave the highest initial capacity (131.5 mA h g^{-1}) and best capacity retention (95% even after 50 cycles) compared to a similar LMO obtained from microwave-assisted sysnthesis[29] (also with $n_{Mn} \approx 3.5+$) that gave poor performance (initial capacity of 118.6 mA h g^{-1}, and 33.2% capacity retention after 50 cycles). Thus, the high-performance of our LMO-ma stems solely from the strategic microwave synthesis protocol. Second, the best-performing LMO and LMOA are those with $n_{Mn} \approx 3.5+$ which were obtained by a pre- or post-annealing microwave irradiation step. Third, all the LMOA samples showed lower discharge capacity but, interestingly, exhibited excellent capacity retention, the microwaved samples giving the highest performance. Fourth, LMO-a (with $n_{Mn} = 3.165+$, capacity retention of 88%) can be optimized or tuned to give $n_{Mn} = 3.5+$ and thus enhanced capacity retention (91%) by subjecting the powder to microwave irradiation. The same phenomenon is also observed for the LMOA-a (with $n_{Mn} = 3.310+$, capacity retention of 92.8%) which gave $n_{Mn} = 3.5$ with enhanced capacity and capacity retention (99.6%). Finally, LMOA-a and LMOA-ma with lower average manganese oxidation state ($n_{Mn} \approx 3.31+$) gave better capacity retention than LMO-am and LMO-ma with higher n_{Mn} values of *ca.* 3.50+ and 3.54+, respectively. Our results largely contradict various reports that predicted that higher capacity retention could be obtained only at $n_{Mn} > 3.50+$.[14,15,42,43] Also, Zhang *et al.*[29] reported that the best performing dual-doped LMO was with $n_{Mn} = 3.571+$. We can infer from our findings that LMO and doped-LMO with $n_{Mn} \approx 3.5+$ with excellent capacity retention can be obtained if microwave irradiation is strategically used in the synthesis step, pre or post-annealing steps. Microwave irradiation at the pre- or the post-annealing steps of the synthesis has different effects on LMO and LMOA. This should be expected since Al-doping inherently changes the chemistry and electrochemistry of the LMO. For example, from the XRD data, there was lattice contraction upon Al-doping (replacement of the redox-active Mn^{3+}) and hence the lower capacities obtained for LMOA compared to LMO.

Conclusions

Hitherto, the average valence (n_{Mn}) of manganese has been known to be the determining factor for capacity retention in $LiMn_2O_4$ and doped-$LiMn_2O_4$ spinel cathode materials for rechargeable lithium ion battery; when the concentration of Mn^{3+} ions exceeds that of Mn^{4+} ions ($n_{Mn} < 3.5+$) capacity fade/ loss becomes prominent, but when $n_{Mn} > 3.5+$ capacity retention is improved. We report, for the first time, the application of microwave irradiation at the pre- and post-annealing steps of the synthesis of $LiAl_xMn_{2-x}O_4$ ($x = 0$ and 0.3) spinel cathode materials with the view to understanding and optimizing the manganese valence number for enhanced capacity retention. We showed that this strategic microwave irradiation can be used to shrink the spinel particles and lattice parameters for improved crystallinity, and tune the Mn^{3+}/Mn^{4+} ratio to obtain $n_{Mn} \approx 3.5+$ for enhanced electrochemical performance. From the results, two parameters, crystal size (as observed by SEM) as well as Mn oxidation state change simultaneously and therefore it still seems difficult to assign the improvement to one of the effects. Simply put, the electrochemistry of LMO and LMOA can be enhanced by tuning the crystal size and manganese valence to *ca.* 3.5+ by strategic microwave irradiation steps, pre- or post-annealing. If microwave irradiation prior to annealing fails to achieve the $n_{Mn} \approx 3.5+$, one can still obtain the $n_{Mn} \approx 3.5+$ by microwave irradiation after annealing. Clearly, microwave irradiation cannot just be used as a mere heat source to achieve fast chemical reaction, but can be used to tune the physico-chemical properties of electrode materials. Thus, this study has the potential to revolutionize how we use microwave irradiation in the preparation of spinel materials and a plethora of materials for energy storage and conversion systems for enhanced performance. One of the important questions that should be answered is: to what extent can the lattice parameters be shrunk and the particle size be controlled by microwave irradiation to provide the optimum average manganese valence for enhanced electrochemical performance? To answer this question and others, the process is being optimized at our laboratory for pilot-scale production.

Acknowledgements

References

1 B. Scrosati, *Electrochim. Acta*, 2000, **45**, 2461–2466.
2 T. Ohzuku and R. J. Brodd, *J. Power Sources*, 2007, **174**, 449–456.
3 J. Amarilla, K. Petrov, F. Pico, G. Avdeev, J. Rojo and R. Rojas, *J. Power Sources*, 2009, **191**, 591–600.

4   B. Dunn, H. Kamath and J. M. Tarascon, *Science*, 2011, **334**, 928–935.

5   J. Tarascon and M. Armand, *Nature*, 2001, **414**, 359–367.

6   M. Armand and J. Tarascon, *Nature*, 2008, **451**, 652–657.

7   G. Amatucci and J. Tarascon, *J. Electrochem. Soc.*, 2002, **149**, K31–K46.

8   K. Kang, Y. S. Meng, J. Breger, C. P. Grey and G. Ceder, *Science*, 2006, **311**, 977–980.

9   P. Ragupathy, *RSC Adv.*, 2014, **4**, 670–675.

10 N. Choi, Z. Chen, S. A. Freunberger, X. Ji, Y. Sun, K. Amine, G. Yushin, L. F. Nazar, J. Cho and P. G. Bruce, *Angew. Chem., Int. Ed.*, 2012, **51**, 9994–10024.

11 S. Lee, Y. Cho, H. Song, K. T. Lee and J. Cho, *Angew. Chem., Int. Ed.*, 2012, **51**, 8748–8752.

12 M. M. Thackeray, Y. Shao-Horn, A. J. Kahaian, K. D. Kepler, E. Skinner, J. T. Vaughey and S. A. Hackney, *Electrochem. Solid-State Lett.*, 1998, **1**, 7–9.

13 M. Qian, J. Huang, S. Han and X. Cai, *Electrochim. Acta*, 2014, **120**, 16–22.

14 S. Martinez, I. Sobrados, D. Tonti, J. Amarilla and J. Sanz, *Phys. Chem. Chem. Phys.*, 2014, **16**, 3282–3291.

15 Q. Tong, Y. Yang, J. Shi, J. Yan and L. Zheng, *J. Electrochem. Soc.*, 2007, **154**, A656–A667.

16 R. Gummow, A. De Kock and M. Thackeray, *Solid State Ionics*, 1994, **69**, 59–67.

17 M. Reddy, M. S. Raju, N. Sharma, P. Quan, S. H. Nowshad, H. Emmanuel, V. Peterson and B. Chowdari, *J. Electrochem. Soc.*, 2011, **158**, A1231–A1236.

18 F. Jiao, J. Bao, A. H. Hill and P. G. Bruce, *Angew. Chem., Int. Ed.*, 2008, **47**, 9711–9716.

19 Y. Shin and A. Manthiram, *Chem. Mater.*, 2003, **15**, 2954–2961.

20 W. Choi and A. J. Manthiram, *J. Electrochem. Soc.*, 2007, **154**, A614–A618.

21 M. A. Kebede, M. J. Phasha, N. Kunjuzwa, L. J. Le Roux, D. Mkhonto, K. I. Ozoemena and M. K. Mathe, *Sustainable Energy Technologies and Assessments*, 2014, **5**, 44–49.

22 M. Nakayama, K. Watanabe, H. Ikuta, Y. Uchimoto and M. Wakihara, *Solid State Ionics*, 2003, **164**, 35–42.

23 H. Yan, X. Huang and L. Chen, *J. Power Sources*, 1999, **81–82**, 647–650.

24 S. Bao, Y. Liang and H. Li, *Mater. Lett.*, 2005, **59**, 3761–3765.

25 P. Ragupathy, H. N. Vasan and N. Munichandraiah, *Mater. Chem. Phys.*, 2010, **124**, 870–875.

26 Y. Fu, C. Lin, Y. Su, J. Jean and S. Wu, *Ceram. Int.*, 2004, **30**, 1953–1959.

27 B. He, W. Zhou, S. Bao, Y. Liang and H. Li, *Electrochim. Acta*, 2007, **52**, 3286–3293.

28 H. Liu, C. Hu, X. Zhu, H. Hao, J. Luo, J. Zhou and S. Ouyang, *Mater. Chem. Phys.*, 2004, **88**, 290–294.

29 H. Zhang, Y. Xu, D. Liu, X. Zhang and C. Zhao, *Electrochim. Acta*, 2014, **125**, 225–231.

30 S. Bao, Y. Liang, W. Zhou, B. He and H. Li, *J. Power Sources*, 2006, **154**, 239–245.

31 S. H. Chang, K. S. Ryu, K. M. Kim, M. S. Kim, I. K. Kim and S. G. Kang, *J. Power Sources*, 1999, **84**, 134–137.

32 H. Chen and D. J. Hsu, *J. Alloys Compd.*, 2014, **598**, 23–26.

33 H. Chen and D. Hsu, Characterization of crednerite-$Cu_{1.1}Mn_{0.9}O_2$ films prepared using sol–gel processing, *Appl. Surf. Sci.*, 2014, **290**, 161–166.

34 E. Elbadraoui, J. Baudour, F. Bouree, B. Gillot, S. Fritsch and A. Rousset, Cation Distribution and Mechanism of Electrical Conduction in Nickel–Copper Manganite Spinels, *Solid State Ionics*, 1997, **93**, 219–225.

35 C. J. Jafta, M. K. Mathe, N. Manyala, W. D. Roos and K. I. Ozoemena, *ACS Appl. Mater. Interfaces*, 2013, **5**, 7592–7598.

36 J. F. Marco, J. R. Gancedo, M. Gracia, J. L. Gautier, E. I. Ríos, H. M. Palmer, C. Greaves and F. J. Berry, *J. Mater. Chem.*, 2001, **11**, 3087–3093.

37 V. Mittal, P. Chandramohan, S. Bera, M. Srinivasan, S. Velmurugan and S. Narasimhan, *Solid State Commun.*, 2006, **137**, 6–10.

38 J. Töpfer, A. Feltz, D. Gräf, B. Hackl, L. Raupach and P. Weissbrodt, *Phys. Status Solidi A*, 1992, **134**, 405–415.

39 T. Yamashita and P. Hayes, *Appl. Surf. Sci.*, 2008, **254**, 2441–2449.

40 M. Reddy, A. Sakunthala, S. SelvashekaraPandian and B. Chowdari, *J. Phys. Chem. C*, 2013, **117**, 9056–9064.

41 X. Zhao, M. Reddy, H. Liu, S. Ramakrishna, G. S. Rao and B. Chowdari, *RSC Adv.*, 2012, **2**, 7462–7469.

42 Y. Shin and A. Manthiram, *J. Electrochem. Soc.*, 2004, **151**, A204–A208.

43 R. J. Gummow, A. de Kock and M. M. Thackeray, *Solid State Ionics*, 1994, **69**, 59–67.